JOURNAL OF MATERIALS SCIENCE 27 (1992) 3173–3180

Interfacial properties of fibrous composites

Part I *Model for the debonding and pull-out processes*

C. Y. YUE*
School of Mechanical and Production Engineering, Nanyang Technological University, Nanyang Avenue, Singapore 2263
W. L. CHEUNG
Department of Mechanical Engineering, University of Hong Kong, Pokfulam Road, Hong Kong

The processes for debonding and pull-out in parallel-sided as well as tapered fibre composites are described. Models which can predict and account for all the reported experimental debonding and pull-out behaviour are developed. The effect of the interfacial properties on the plot of maximum pull-out force against fibre embedded length is elucidated. Knowledge of the interfacial parameters of a composite allows proper characterization and leads to better prediction of the mechanical properties.

1. Introduction

The strength and toughness of fibrous composites are dependent on the interfacial properties [1] which include both the parameters which characterize the interface, and the physical nature of the interface. This is why there is much ongoing interest in the interfacial properties in different composite systems. The present work is concerned with the former aspect of interfacial studies, and is the second report on the interfacial properties of glass-reinforced polypropylene (PP). The latter aspect of interfacial properties, concerning the character and nature of both silane-treated glass fibre and clean untreated glass fibre-reinforced PP, has already been considered in earlier reports [2, 3].

The pull-out test is widely used [1] for determining interfacial parameters such as the matrix shrinkage pressure on the fibre, P_o, the interfacial coefficient of friction, μ, and the interfacial shear strength, τ_i. The strength of the composite is controlled by the interfacial shear strength, while the toughness is influenced by the matrix shrinkage pressure, P_o, and the interfacial coefficient of friction, μ. The value of τ_i is usually estimated from the single-fibre pull-out test. However, pull-out tests on specimens which are subjected to external hydrostatic pressures [4, 5] must be conducted in order to determine μ and P_o. Although the pull-out test is so commonly used, there is no clear understanding of the effect of interfacial properties such as interfacial shear strength, Poisson shrinkage of the fibre and interfacial friction on the resulting force–displacement curve, and the plot of debonding force against fibre-embedded length.

The debonding criterion adopted affects the interpretation of pull-out test data. The debonding stress in a single-fibre pull-out has been interpreted in terms of either a maximum interfacial shear stress criterion [6–8] or an interfacial fracture criterion [9–12]. The validity of either a strength-based or fracture-based approach to a given system can be determined [10] through pull-out tests on specimens with different fibre diameters. It has been shown for a glass fibre–PP system [12] that both approaches are applicable when the fibre diameter is less than 400 μm, and that the strength-based approach is more appropriate for larger fibre diameters. The choice of the appropriate debonding criterion is necessary for reliable prediction of the force, F_i, at which debonding occurs in the composite.

The existing debonding criteria cannot explain some of the reported experimental observations on the interfacial debonding phenomenon. These include the two-stage debonding process [13] and the change in position of debonding crack initiation in different pull-out systems [14, 15]. It is possible that the point at which interfacial failure initiates depends not only on the interfacial properties but also on the properties of the fibre and matrix, and the test configuration. This has not been discussed in previous studies.

In the present study, a strength-based approach will be adopted for the single-fibre pull-out test. The interfacial shear stress distribution along the embedded fibre will be analysed and a theory of interfacial debonding will be developed. It will be shown that the model developed can account for all reported experimental observations on the interfacial debonding phenomenon. Secondly, the theoretical aspects of the pull-out test of a slightly tapered fibre will be considered and a model will be developed. The applicability of the pull-out model is evaluated using experimental data. It will be shown in a following report that on the basis of the models developed, the interfacial parameters P_o, μ and τ_i, can be determined from

* To whom correspondence should be addressed.

0022–2461

one set of data from slightly tapered fibre pull-out specimens.

2. The debonding process

2.1. Interfacial shear stress distribution

Consider the application of a load to a fully supported pull-out specimen as shown in Fig. 1. The load is applied through gripping the opposing ends of the specimen at the free end of the fibre and the region of the matrix away from the embedded fibre. The stress across the fibre end is assumed to be negligible. Under the action of a pull-out force F_p, the specimen displaces elastically as shown in Fig. 2. The shear force on the fibre element dx is equal to $2\pi r\tau_x dx$. Assuming that the shear force decreases linearly in the y direction such that it is zero at the circumferential surface of the matrix block and adopting a shear-lag analysis, the following expression (see Appendix) for the interfacial shear stress distribution can be derived [16]:

$$\tau_x = \frac{F_p}{2\pi r}\left[\alpha(1-\psi)\exp(-\alpha x) + \alpha\cosh\alpha x\,\frac{\psi + (1-\psi)\exp(-\alpha L)}{\sinh\alpha L}\right] \quad (1)$$

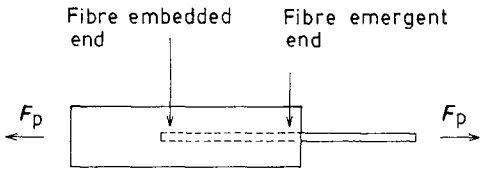

Figure 1 Schematic diagram of single-fibre pull-out test considered.

where

$$\alpha = \left[\frac{2G_m}{\{[r_m/(r_m-r)]\ln(r_m/r) - 1\}(r_m^2 - r^2)} \times \left(\frac{E_m(r_m^2 - r^2) + E_f r^2}{r^2 E_f E_m}\right)\right]^{1/2}$$

$$\psi = \frac{E_m(r_m^2 - r^2)}{E_m(r_m^2 - r^2) + E_f r^2}$$

and x is the distance from the fibre embedded end, G_m and r_m are the shear modulus and radius of the matrix block, respectively, and E_m and E_f are the modulus of the matrix and fibre, respectively.

2.2. Position of interfacial crack initiation

The effect of the relative modulus of the matrix and fibre (E_f/E_m), and the influence of the specimen dimension (relative size of the matrix and the fibre, r_m/r) on the interfacial shear stress distribution will now be examined. Consider pull-out specimens of the same dimensions for the two different matrix systems as in Table I. The interfacial shear stress distributions in the above two systems under the action of a pull-out force of 10 N are as depicted in Fig. 3.

It can be seen from Fig. 3 that the interfacial shear stress in the composite system with the smaller ratio of E_f/E_m (glass fibre–PP system) changes drastically along the fibre (see curve (a)). The interfacial shear stress concentration in this system exists at the emergent end of the fibre. In contrast, the interfacial shear stress distribution in the system with the larger ratio of E_f/E_m (glass fibre–rubber system) is relatively even and the stress concentration is located at the fibre

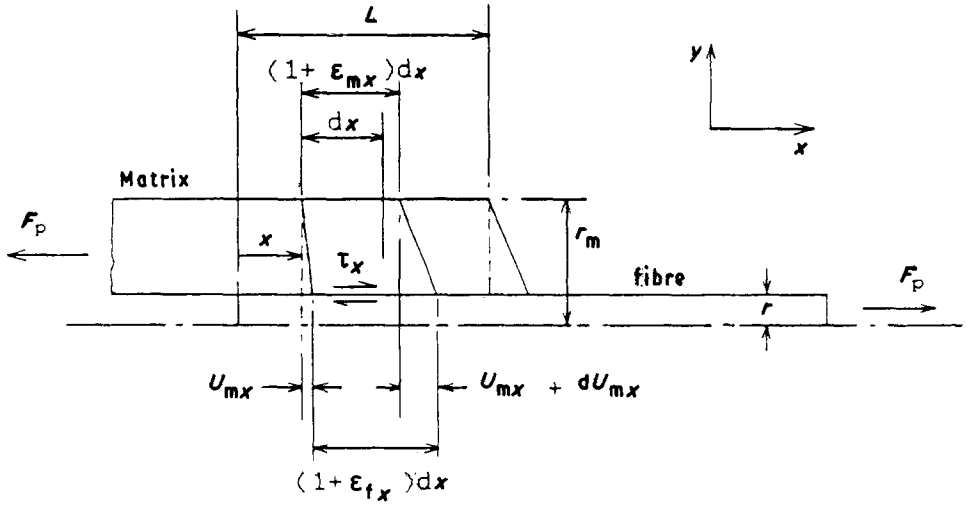

Figure 2 Elastic displacement of the fibre–matrix interface under a load.

TABLE I Parameters of composite systems considered in the analysis of τ_x

System	E_m (GPa)	E_f (GPa)	ν_m	ν_f	r_m (mm)	r (mm)	L (mm)
Glass fibre–PP	1.4	60.0	0.35	0.22	2.5	0.1	10
Glass fibre–rubber	0.002	60.0	0.5	0.22	2.5	0.1	10

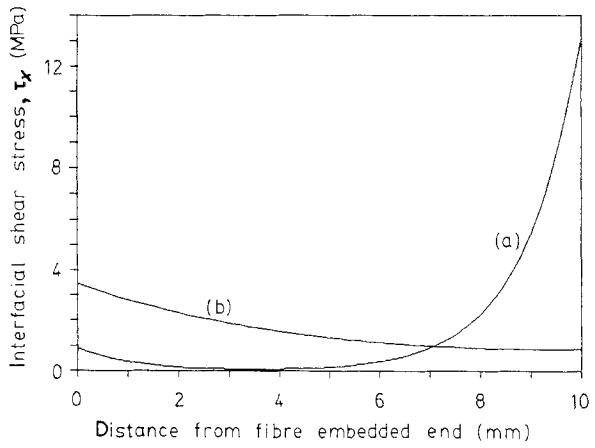

Figure 3 Interfacial shear stress distribution at $F_p = 10$ N in (a) glass fibre–PP system, (b) glass fibre–rubber system.

embedded end of the fibre (see curve (b)). This indicates that the point of the interfacial crack initiation in the pull-out specimen is dependent on the relative modulus ratio of the matrix and fibre.

The effect of the relative size of the fibre and the matrix (r_m/r) will now be considered. Fig. 4 shows the variation of the interfacial shear stress, τ_x, at the embedded end (curve (a)) and emergent end (curve (b)) of the fibre with radius of the matrix block, r_m, for the glass fibre–PP system in Table I. The radius of the fibre in the system is assumed to be constant. It can be seen that when r_m/r is small (i.e. small r_m), the interfacial shear stress at the embedded end of the fibre is higher than that at the emergent end. The interfacial shear stress at both the emergent end and the embedded end are equal when r_m/r is equal to 8 ($r_m = 0.8$ mm). However, for larger values of r_m/r (for $r_m > 0.8$ mm), the interfacial shear stress at the emergent end of the fibre is much larger than that at the embedded end. This can be attributed to the rapid decrease in τ_x at the embedded end such that τ_x becomes very small when r_m/r is large. In contrast, τ_x at the emergent end of the fibre increases to a maximum before decreasing slowly as r_m is increased.

It is apparent from the above analysis that the position of debonding crack initiation can occur at either the emergent or the embedded end of the fibre, depending on the relative modulus of the fibre and matrix, and on the relative diameters of the fibre and matrix utilized in the pull-out specimen. This accounts for the earlier reports of debonding crack initiation at either the emergent or the embedded end of the fibre in different composite systems. Therefore although debonding crack initiation in most systems has been reported to occur at the emergent end, debonding crack initiation in a steel wire–rubber system [14] which has a high E_f/E_m occurs, as expected, at the embedded end of the fibre.

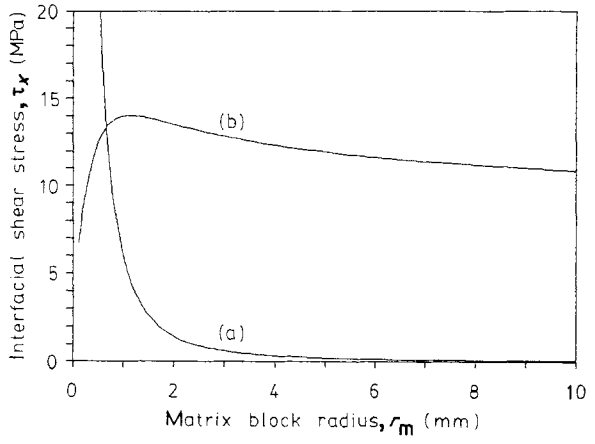

Figure 4 Variation of interfacial shear stress at: (a) fibre embedded end, and (b) fibre emergent end, with radius of matrix block for the glass fibre–PP system at $F_p = 10$ N.

2.3. Pull-out force for interfacial debonding

Consider the more general case where E_f/E_m is small such that the maximum interfacial shear stress exists at the emergent end of the fibre. Assuming a maximum shear stress criterion, the crack will initiate when τ_x reaches the critical interfacial shear stress τ_i. From Equation 1, it can be seen that the pull-out force for crack initiation, F_i, is

$$F_i = 2\pi r\tau_i\left[\alpha(1-\psi)\exp(-\alpha L) + \frac{[\psi+(1-\psi)\exp(-\alpha L)]\alpha\cosh(\alpha L)}{\sinh(\alpha L)}\right]^{-1} \quad (2)$$

After crack initiation, there will be a redistribution of stresses at the interface. Further crack propagation will occur only if the shear stress at the crack tip is again increased to τ_i through an increase in the applied load. In the present analysis, crack initiation is assumed to lead to partial debonding. This assumption is valid for many composite systems. However, in some systems, catastrophic complete debonding occurs after crack initiation.

2.4. Maximum pull-out force F_d

Frequently in many composite systems, the debonding crack initiates in the specimen well before it reaches the maximum pull-out force F_d on the load–extension plot of a pull-out test. Thus both a debonded and "bonded" region exist even before F_d is reached. For the crack to propagate further, the applied force must overcome the load that can be sustained in the debonded region and be sufficiently large so that the maximum shear stress at the crack tip will once more approach τ_i. This is the case in a glass fibre–PP system [2]. Therefore, F_d in these systems has two components.

If the debonding crack has travelled through a distance l_d (see Fig. 5), the fibre embedded length L

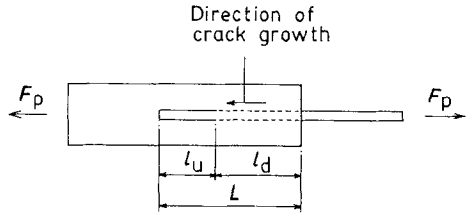

Figure 5 Schematic diagram of partially debonded pull-out specimen: l_u = bonded region, l_d = debonded region.

will consist of the bonded region ($0 < x < l_u$) and the debonded region ($l_u < x < L$). The shear stress distribution in the bonded region is governed by Equation 1 but the bonded region has decreased from L to l_u. For crack growth to continue, the shear stress at the crack front must be equal to τ_i and the applied force required, F_{uy}, to achieve this is

$$F_{uy} = 2\pi r\tau_i\left[\alpha(1-\psi)\exp(-\alpha l_u) + \frac{[\psi+(1-\psi)\exp(-\alpha l_u)]\alpha\cosh(\alpha l_u)}{\sinh(\alpha l_u)}\right]^{-1} \quad (3)$$

In the debonded region, the applied force F_p has to act against the interfacial friction between the fibre and the matrix. For a rigid fibre system, the total frictional force F_f in the debonded length l_d is given by

$$F_f = 2\pi r P_o \mu (L - l_u) \quad (4)$$

The pull-out force F_p on the specimen is the sum of the force in the bonded region F_{uy} and the force in the debonded region F_f such that

$$F_p = F_{uy} + F_f \quad (5)$$

Fig. 6 shows the variations of F_p, F_{uy} and F_f as the debonding crack propagates along the fibre. Once the debonding crack has initiated and begun to grow, F_{uy} will drop due to shortening of the debonded length l_u. However, the corresponding increase in the debonded region l_d gives rise to an increase in the interfacial friction F_f. If the embedded length of the fibre is long, F_{uy} is a slow function of the debonding crack length during the initial stage of crack growth. The pull-out force F_p will increase from $F_p = F_i$ at the point of debonding crack initiation ($l_d = 0$) to $F_p = F_d$ at a rate corresponding to the rate of increase in interfacial friction due to debonding crack propagation.

The rate of increase in F_f is equal to the rate of decrease in F_{uy} at $l_u = L_c$, where L_c is the critical embedded length at which the pull-out force F_p attains a maximum value F_d. If the parameters of the pull-out system are known, L_c can be calculated from Equation 5 by taking $dF_p/dl_u = 0$. It has been shown [16] that L_c is dependent on almost all the system parameters but is independent of the embedded length L.

When the debonding crack front displacement has propagated beyond L_c, the rate of increase in F_f is smaller than the rate of decrease in F_{uy}. At some stage, crack growth will change from steady to catastrophic in nature such that the remaining bonded region fails without further increase in F_p (see Fig. 6). The fibre will then begin to pull out. Hence, the maximum pull-out force F_d occurs at $l_u = L_c$ where

$$F_d = F_{uy} + 2\pi r P_o \mu (L - L_c) \quad (6)$$

2.5. Relation between F_d and the fibre embedded length L

It is common to plot the pull-out force F_d against the embedded length L for test data from a single-fibre pull-out experiment. Two situations exist in the pull-out tests. For specimens with $L < L_c$, the value of F_{uy} required to maintain the shear stress at the crack front at the critical value τ_i will drop rapidly once the debonding crack has initiated and begun to grow. Complete debonding occurs catastrophically without further increase in the pull-out force. Therefore, the pull-out force for complete debonding is equal to the force for debonding crack initiation in Equation 2.

For specimens with $L \gg L_c$, F_{uy} is a slow function of the crack length during the early stage of crack growth (see curve (a) in Fig. 6). As the interfacial crack propagates, the increase in the interfacial frictional force F_f with debonded length l_d will cause the shear stress at the crack front to drop below τ_i. Hence, the applied load on the system must be increased for debonding to progress further. In a rigid fibre system, the extra load required to cause complete debonding is equal to $2\pi r P_o \mu (L - L_c)$. It can be seen that this extra load varies linearly with L.

2.5.1. Effect of interfacial shear strength τ_i

Fig. 7 shows the effect of interfacial strength τ_i on the shape of the curve of F_d against L. For a system with high interfacial strength τ_i, the curve exhibits a distinctive bend at $L = L_c$ (see curve (a)). As τ_i decreases the curve shifts downward (see curve (b)). If τ_i is only marginally higher than the interfacial frictional stress

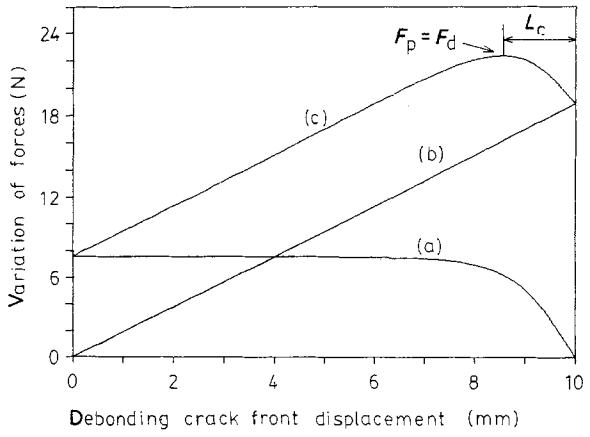

Figure 6 Variation of (a) F_{uy}, (b) F_f and (c) F_p with the debonding crack length.

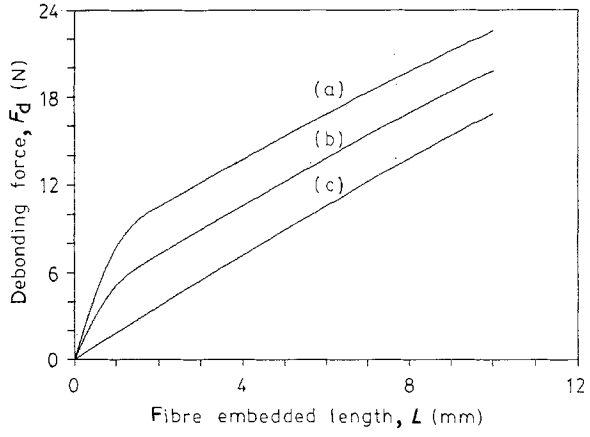

Figure 7 Theoretical plot of F_d against L for glass fibre–PP system for (a) $\tau_i = 15$ MPa, (b) $\tau_i = 10$ MPa, (c) $\tau_i = \tau_f$.

τ_f, the curve almost becomes a straight line which passes through the origin (see curve (c)).

In a fibre pull-out experiment, the pull-out data for $L < L_c$ may be difficult to obtain due to practical limitations. It is therefore possible that the experimental results appear as a relatively straight curve which intercepts the vertical axis at a point above the origin. Such a case has been reported [17] but the intercept on the vertical axis was attributed to matrix residue attached to the emergent end of the extracted fibre. However, the present analysis clearly shows that the intercept on the F_d axis might partly be due to the dynamics of interfacial debonding as represented by curve (a) in Fig. 7.

2.5.2. Effect of Poisson shrinkage of fibre

If a ductile fibre is used or if the aspect ratio of the embedded fibre is very large, the Poisson shrinkage effect becomes significant. Under these conditions high stresses exists in the fibre when the system is loaded. The Poisson shrinkage in the fibre reduces the effective radial pressure. Hence, the frictional force on the debonded region will drop. Consequently, the rate of increase in F_d will no longer be linear but will diminish with increasing L. It has been shown [16] that under these conditions, the pull-out force F_d becomes

$$F_d = \frac{\pi r^2 P_o}{R} + \left(F_{uy} - \frac{\pi r^2 P_o}{R}\right) \times \exp\left(\frac{-2\mu R(L - L_c)}{r}\right) \quad (7)$$

where $R = E_m \nu_f / [E_f(1 + \nu_m)]$, and ν_f and ν_m are the Poisson's ratios of the fibre and matrix, respectively.

Fig. 8 shows the theoretical curves of F_d versus L with (curve (b)) and without (curve (a)) the effect of Poisson shrinkage on the fibre for the glass fibre–PP system in Table I. It is evident that the effect of the Poisson shrinkage is to decrease the slope of the later portion of the curve. In addition, the deviation of the curves increases at large embedded fibre lengths where the debonding force F_d is necessarily higher.

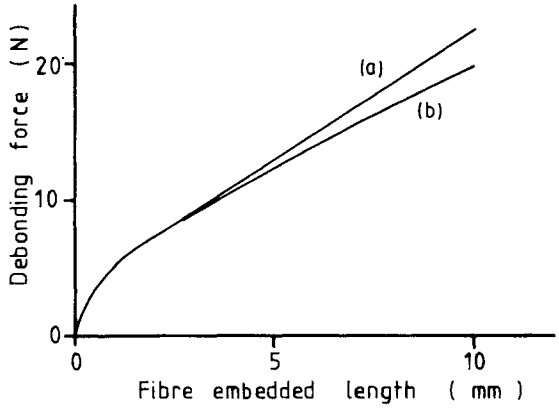

Figure 8 Effect of Poisson shrinkage of fibre on plot of F_d against L: (a) without Poisson shrinkage, (b) with Poisson shrinkage.

2.5.3. Effect of interfacial friction

Fig. 9 shows the effect of the interfacial frictional stress τ_f on the plot of F_d against L for the glass fibre–PP system in Table I. In practice, the interfacial shear stress is dependent on the nature of the interface or interphase, and on the surface properties of the surfaces in sliding contact. It is apparent that the slope of the plot beyond the "knee" at $L = L_c$ increases with increasing τ_f.

For a given fibre embedded length $L > L_c$, F_d is larger for the system with higher τ_f (see Fig. 9). This is in agreement with the results obtained elsewhere [4, 5] where τ_f in the systems considered was increased via the application of external pressure on the specimens during pull-out.

3. The pull-out process

3.1. Development of model

A schematic representation of a single-fibre pull-out specimen which contains a slightly tapered fibre in the matrix is shown in Fig. 10. The fibre is assumed to be rigid while the matrix is ductile. The degree of taper of the fibre is defined by $\tan\theta$ where

$$\tan\theta = \frac{(D_1 - D_2)}{2s} \quad (8)$$

and D_1 and D_2 are the fibre diameters at the embedded end and emergent end of the fibre, respectively, and s is

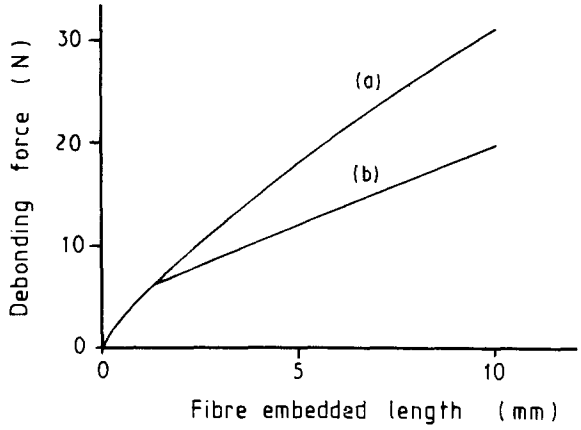

Figure 9 Predicted plots of F_d against L for the glass fibre–PP system assuming $\tau_i = 10$ MPa and (a) $\tau_f = 6$ MPa, (b) $\tau_f = 3$ MPa.

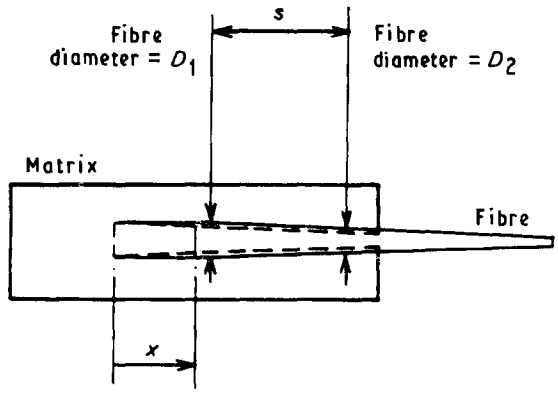

Figure 10 Schematic representation of test on a slightly tapered single-fibre pull-out specimen.

the distance between D_1 and D_2; $\tan\theta$ can either be positive or negative.

Consider the general case in Fig. 10. The radial pressure on the fibre before debonding can be assumed to be constant along the embedded length and equal to the matrix shrinkage pressure P_o. After debonding, the relative movement between the fibre and the matrix will increase the radial pressure on the fibre. The change in radial pressure is dependent on the modulus of the matrix, the fibre geometry, and the pull-out displacement. When the fibre has been displaced by a distance x, the radial expansion Δ of the cavity in contact with the fibre is $\Delta = x\tan\theta$. The corresponding radial strain in the matrix around the cavity becomes

$$\frac{\Delta}{r} = x\frac{\tan\theta}{r} \tag{9}$$

This strain introduces an increase in the radial pressure, δp, on the fibre. If the size of the matrix block is considerably larger than the fibre diameter, then thick-walled cylinder theory is applicable and δp is given by

$$\delta p = \frac{\Delta E_{mc}}{r(1 + \nu_m)} \tag{10}$$

where E_{mc} is the compressive modulus of the matrix material. Substituting Equation 9 into Equation 10 gives

$$\delta p = x\frac{E_{mc}\tan\theta}{r(1 + \nu_m)} \tag{11}$$

The radial pressure may either increase or decrease with the pull-out displacement since the degree of taper of the fibre can either be positive ($D_1 > D_2$) or negative ($D_1 < D_2$). In the case of a fibre of constant diameter ($\tan\theta = 0$), the radial pressure remains unchanged during fibre pull-out.

3.2. Frictional pull-out stress

It can readily be shown [16] that the frictional pull-out stress, σ_p, in a specimen with a fibre of constant diameter is

$$\sigma_p = \frac{P_o}{R}\left[1 - \exp\left(\frac{-2\mu R(L - x)}{r}\right)\right] \tag{12}$$

where $R = E_{mc}\nu_f/[E_f(1 + \nu_m)]$. The form of Equation 12 is similar to that given elsewhere [18]. In the case of a tapered fibre, Equation 12 should be modified to account for the increase in radial pressure so that σ_p becomes

$$\sigma_p = \frac{P_o + \delta p}{R}\left[1 - \exp\left(\frac{-2\mu R(L - x)}{r}\right)\right] \tag{13}$$

The complete expression for σ_p can be obtained by substituting Equation 11 into Equation 13.

3.3. Shape of pull-out curves

The use of tapered fibres gives rise to a variety of pull-out curves. Theoretical curves of the frictional pull-out stress σ_p against the fibre displacement x for specimens with different values of $\tan\theta$ can readily be generated using Equation 13 since the terms in the equation are related to the specimen geometry and the physical properties of the composite system. The theoretical curves for specimens with different $\tan\theta$ for the glass fibre–PP system in Table I are as shown in Fig. 11. To generate the curves in Fig. 11, the values of P_o and μ were assumed to be 10 MPa and 0.3, respectively. These assumed values are reasonable since they are close to the values of P_o (7 MPa) and μ (0.6) in a steel wire–polycarbonate system [19].

It can be seen from Fig. 11 that a positive $\tan\theta$ may cause σ_p to increase to a maximum before gradually decreasing to zero as pull-out progresses (curve (b)). If the value of $\tan\theta$ is large enough, it is possible for σ_p to increase to a value equal to the tensile strength, σ_{fu}, of the fibre. Therefore, the fibre will break at $\sigma_p = \sigma_{fu}$ and the pull-out force will drop sharply to zero (see curve (a)). In contrast, a large negative $\tan\theta$ may cause loss of contact between the fibre and the matrix before the fibre is completely extracted from the matrix. As a result, σ_p will drop to zero at a point where $x < L$ (see curve (e)). All the predicted pull-out curves in Fig. 11 have been observed experimentally [20].

3.4. Work expended during pull-out

The work done against frictional pull-out, W, is represented by the area under the pull-out curve where

$$W = \int_0^L \pi r^2 \sigma_p \, dx$$

Substituting Equation 13 into the above equation

$$W = \int_0^L \left(\pi\frac{r^2}{R}\right)\left(P_o + x\frac{E_{mc}\tan\theta}{r(1 + \nu_m)}\right) \times\left[1 - \exp\left(\frac{-2\mu R(L - x)}{r}\right)\right]dx \tag{14}$$

It can be shown [16] that the solution to the above integral is

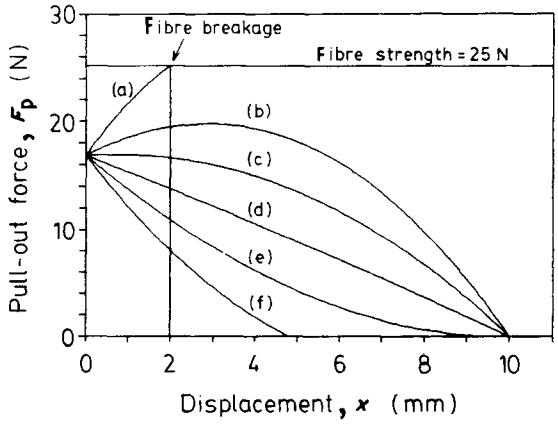

Figure 11 Theoretical curves of pull-out force against displacement based on Equation 13 for glass fibre–PP system: $\tan\theta$ = (a) 4×10^{-4}, (b) 2×10^{-4}, (c) 1×10^{-4}, (d) 0, (e) -1×10^{-4}, (f) -2×10^{-4}.

$$W = \frac{\pi r^2}{R}\left(P_o L - \frac{P_o r}{2\mu R}\left[1 - \exp\left(\frac{-2\mu RL}{r}\right)\right] + \frac{E_{mc}\tan\theta}{r(1+\nu_m)}\left\{\frac{L^2}{2} - \frac{rL}{2\mu R} + \left(\frac{r}{2\mu R}\right)^2 \times \left[1 - \exp\left(\frac{-2\mu RL}{r}\right)\right]\right\}\right) \quad (15)$$

For a specimen with an embedded fibre of constant diameter $\tan\theta = 0$, the work done against frictional pull-out reduces to W_o where

$$W_o = \frac{\pi r^2}{R}\left\{P_o L - \frac{P_o r}{2\mu R}\left[1 - \exp\left(\frac{-2\mu RL}{r}\right)\right]\right\} \quad (16)$$

The difference in work done against frictional pull-out between a specimen with a slightly tapered fibre and one with a fibre of constant diameter can be found by subtracting Equation 16 from Equation 15, giving

$$W - W_o = \frac{\pi r E_{mc}\tan\theta}{R(1+\nu_m)}\left\{\frac{L^2}{2} - \frac{rL}{2\mu R} + \left(\frac{r}{2\mu R}\right)^2 \times \left[1 - \exp\left(\frac{-2\mu RL}{r}\right)\right]\right\} \quad (17)$$

The term $(W - W_o)$ is the shaded area of the pull-out portion of the load–displacement plot shown in Fig. 12. As expected, slightly tapered fibres with positive values of $\tan\theta$ increase the work expended during pull-out. It will be shown in a subsequent paper that the interfacial parameters can be calculated from the expression for $(W - W_o)$.

4. Conclusion

A debonding model for evaluating the stresses at the fibre in a pull-out configuration has been developed. The model, which assumes a maximum shear stress criterion, can account for all the different reported experimental observations on the debonding crack initiation phenomenon. The model reveals how the plot of maximum debonding pull-out force is affected by the interfacial strength, Poisson shrinkage of the fibre, and interfacial frictional force. A pull-out model has also been developed to describe the pull-out process in specimens which may not have fibres of constant diameter. There is also experimental support for the latter model.

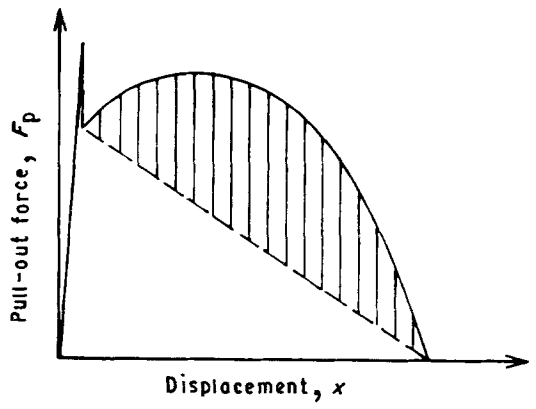

Figure 12 Extra frictional work done (shaded area) due to pull-out of a slightly tapered fibre, $\tan\theta > 0$.

Appendix: Longitudinal stress distribution at the interface

Consider the application of a load to the specimen in Fig. 1. The radius of the cylindrical matrix block is r_m and the radius of the fibre is r. The specimen will be displaced elastically as shown in Fig. 2. Neglecting the stress across the fibre end, it can be shown from displacement considerations that

$$(1 + \varepsilon_{mx})dx + du_{mx} = (1 + \varepsilon_{fx})dx$$

$$\frac{du_{mx}}{dx} = \varepsilon_{fx} - \varepsilon_{mx} \quad (A1)$$

Next consider the stresses acting on an element of the fibre and of the matrix at the interface of the pull-out specimen (Fig. A1). From the equilibrium of the forces at the interface

$$\pi(r_m^2 - r^2)d\sigma_{mx} = -2\pi r\tau_x dx$$

Therefore

$$\tau_x = -\left(\frac{r_m^2 - r^2}{2r}\right)\frac{d\sigma_{mx}}{dx} \quad (A2)$$

For the fibre element, one can equate $\pi r^2 d\sigma_{fx} = 2\pi r\tau_r dx$, so

$$\tau_x = \frac{r}{2}\left(\frac{d\sigma_{fx}}{dx}\right) \quad (A3)$$

For any cross-section at x (see Fig. 2), the pull-out force can be written as

$$F_p = \pi(r_m^2 - r^2)\sigma_{mx} + \pi r^2\sigma_{fx} \quad (A4)$$

From Fig. 2, the displacement U_{mx} can be written as

$$U_{mx} = \int_r^{r_m}\frac{\tau_y}{G_m}dy \quad (A5)$$

where τ_y is the matrix shear stress in the y direction and G_m is the shear modulus of the matrix. The shear force, S_i, on the element of the matrix at the interface is $S_i = 2\pi r\tau_x dx$. Since the pull-out specimen is gripped at the end of the matrix block, no shear force therefore acts on its circumferential surface. Assuming the shear force decreases linearly in the y-direction from S_i at the interface to zero at the circumferential surface of the matrix block, the shear stress across the matrix, τ_y, becomes

$$\tau_y = \tau_x\frac{r}{y}\left(\frac{r_m - y}{r_m - r}\right)$$

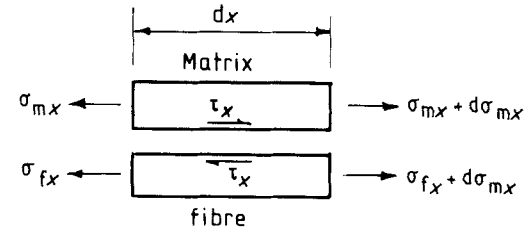

Figure A1 Stress distributions at the interface.

Substituting the above equation into Equation A5 and integrating,

$$U_{mx} = \frac{r\tau_x}{G_m}\left[\left(\frac{r_m}{r_m - r}\right)\ln\left(\frac{r_m}{r}\right) - 1\right] \quad (A6)$$

Differentiating Equation A6 with respect to x,

$$\frac{dU_{mx}}{dx} = \frac{r}{G_m}\left[\left(\frac{r_m}{r_m - r}\right)\ln\left(\frac{r_m}{r}\right) - 1\right]\frac{d\tau_x}{dx} \quad (A7)$$

Differentiating Equation A2 with respect to x,

$$\frac{d\tau_x}{dx} = -\left(\frac{r_m^2 - r^2}{2r}\right)\frac{d^2\sigma_{mx}}{dx^2} \quad (A8)$$

From Equations A8, A7 and A4, and applying Hooke's law to the strains ε_{fx} and ε_{mx} in Equation A1, it can be shown that

$$\frac{d^2\sigma_{mx}}{dx^2} = K_a\sigma_{mx} + C_a \quad (A9)$$

where K_a and C_a are constants denoted by

$$K_a = 2G_m\left[\left(\frac{r_m}{r_m - r}\right)\ln\left(\frac{r_m}{r}\right) - 1\right]^{-1} \times (r_m^2 - r^2)^{-1}\left(\frac{E_m(r_m^2 - r^2) + E_f r^2}{r^2 E_f E_m}\right)$$

$$C_a = -2G_m F_p\left[\left(\frac{r_m}{r_m - r}\right)\ln\left(\frac{r_m}{r}\right) - 1\right]^{-1} \times (r_m^2 - r^2)^{-1}(\pi r^2 E_f)^{-1}$$

Equation A9 is a second-order differential equation which can readily be solved. It can be shown [16] that the solution is

$$\sigma_{mx} = \frac{F_p}{(r_m^2 - r^2)\pi}\left\{\psi + (1 - \psi)\exp(-\alpha x) - [\psi + (1 - \psi)\exp(-\alpha L)]\frac{\sinh(\alpha x)}{\sinh(\alpha L)}\right\} \quad (A10)$$

where

$$\alpha = K_a^{1/2}$$

and

$$\psi = \frac{E_m(r_m^2 - r^2)}{E_m(r_m^2 - r^2) + E_f r^2}$$

Differentiating Equation A10 with respect to x and substituting into Equation A2 yields

$$\tau_x = \frac{F_p}{2\pi r}\left\{\alpha(1 - \psi)\exp(-\alpha x) + [\psi + (1 - \psi)\exp(-\alpha L)]\frac{\alpha\cosh(\alpha x)}{\sinh(\alpha L)}\right\} \quad (A11)$$

The expression for the tensile stress on the fibre is

$$\sigma_{fx} = \frac{F_p}{\pi r^2}\left[1 - \left(\psi + (1 - \psi)\exp(-\alpha x) - \frac{[\psi + (1 - \psi)\exp(-\alpha L)]\sinh(\alpha x)}{\sinh(\alpha L)}\right)\right] \quad (A12)$$

Therefore, the average tensile stress on the matrix σ_{mx}, the shear stress at the interface τ_x, and the average tensile stress on the fibre σ_{fx} are governed by Equations A10, A11 and A12, respectively.

References

1. C. Y. YUE and W. L. CHEUNG, *J. Mater. Sci.* **27** (1992) 3181.
2. *Idem, ibid.* **26** (1991) 870.
3. W. L. CHEUNG and C. Y. YUE, *Polym. Commun.* **31** (1990) 96.
4. P. B. BOWDEN, *J. Mater. Sci.* **5** (1970) 517.
5. P. S. CHUA and M. R. PIGGOTT, *Compos. Sci. Tech.* **22** (1985) 185.
6. A. KELLY and W. R. TYSON, *J. Mech. Phys. Solids* **13** (1965) 329.
7. G. A. COOPER, *J. Mater. Sci.* **5** (1970) 645.
8. P. LAWRENCE, *ibid.* **7** (1972) 1.
9. C. GURNEY and J. HUNT, *Proc. R. Soc.* **A299** (1967) 508.
10. J. K. WELLS and P. W. R. BEAUMONT, *J. Mater. Sci.* **23** (1988) 1274.
11. H. STANG and S. P. SHAH, *ibid.* **21** (1986) 953.
12. C. Y. YUE and W. L. CHEUNG, *J. Mater. Sci. Lett.* **10** (1991) 1335.
13. B. BETZ, *J. Mater. Sci.* **17** (1982) 691.
14. A. N. GENT, G. S. FIELDING-RUSSELL, D. I. LIVINGSTON and D. W. NICHOLSON, *ibid.* **16** (1981) 949.
15. J. BOWLING and G. W. GROVES, *ibid.* **14** (1979) 431.
16. W. L. CHEUNG, PhD thesis, University of Hong Kong (1990).
17. P. S. CHUA and M. R. PIGGOTT, *Compos. Sci. Tech.* **22** (1985) 107.
18. *Idem, ibid.* **22** (1985) 33.
19. N. HADJIS and M. R. PIGGOTT, *J. Mater. Sci.* **12** (1977) 358.
20. C. Y. YUE and W. L. CHEUNG, in Proceedings of 7th International Conference on Deformation, Yield and Fracture of Polymers, Churchill College, Cambridge, UK, April 1988 (Plastics and Rubber Institute, London, 1988) p. 84.1.

Received 16 January
and accepted 7 June 1991